EUROPEAN LABORATORY FOR PARTICLE PHYSICS

CERN-PPE/97-094
24th July 1997

Spin alignment of leading $K^*(892)^0$ mesons in hadronic Z^0 decays

The OPAL Collaboration

Abstract

Helicity density matrix elements for inclusive $K^*(892)^0$ mesons from hadronic Z^0 decays have been measured over the full range of K^{*0} momentum using data taken with the OPAL experiment at LEP. A preference for occupation of the helicity zero state is observed at all scaled momentum x_p values above 0.3, with the matrix element ρ_{00} rising to 0.66 ± 0.11 for $x_p > 0.7$. The values of the real part of the off-diagonal element ρ_{1-1} are negative at large x_p, with a weighted average value of -0.09 ± 0.03 for $x_p > 0.3$, in agreement with new theoretical predictions based on Standard Model parameters and coherent fragmentation of the $q\bar{q}$ system from the Z^0 decay. All other helicity density matrix elements measured are consistent with zero over the entire x_p range. The K^{*0} fragmentation function has also been measured and the total rate determined to be $0.74 \pm 0.02 \pm 0.02$ $K^*(892)^0$ mesons per hadronic Z^0 decay.

To be submitted to Physics Letters B

The OPAL Collaboration

K. Ackerstaff[8], G. Alexander[23], J. Allison[16], N. Altekamp[5], K.J. Anderson[9], S. Anderson[12], S. Arcelli[2], S. Asai[24], D. Axen[29], G. Azuelos[18,a], A.H. Ball[17], E. Barberio[8], T. Barillari[2], R.J. Barlow[16], R. Bartoldus[3], J.R. Batley[5], S. Baumann[3], J. Bechtluft[14], C. Beeston[16], T. Behnke[8], A.N. Bell[1], K.W. Bell[20], G. Bella[23], S. Bentvelsen[8], S. Bethke[14], O. Biebel[14], A. Biguzzi[5], S.D. Bird[16], V. Blobel[27], I.J. Bloodworth[1], J.E. Bloomer[1], M. Bobinski[10], P. Bock[11], D. Bonacorsi[2], M. Boutemeur[34], B.T. Bouwens[12], S. Braibant[12], L. Brigliadori[2], R.M. Brown[20], H.J. Burckhart[8], C. Burgard[8], R. Bürgin[10], P. Capiluppi[2], R.K. Carnegie[6], A.A. Carter[13], J.R. Carter[5], C.Y. Chang[17], D.G. Charlton[1,b], D. Chrisman[4], P.E.L. Clarke[15], I. Cohen[23], J.E. Conboy[15], O.C. Cooke[8], M. Cuffiani[2], S. Dado[22], C. Dallapiccola[17], G.M. Dallavalle[2], R. Davis[30], S. De Jong[12], L.A. del Pozo[4], K. Desch[3], B. Dienes[33,d], M.S. Dixit[7], E. do Couto e Silva[12], M. Doucet[18], E. Duchovni[26], G. Duckeck[34], I.P. Duerdoth[16], D. Eatough[16], J.E.G. Edwards[16], P.G. Estabrooks[6], H.G. Evans[9], M. Evans[13], F. Fabbri[2], M. Fanti[2], A.A. Faust[30], F. Fiedler[27], M. Fierro[2], H.M. Fischer[3], I. Fleck[8], R. Folman[26], D.G. Fong[17], M. Foucher[17], A. Fürtjes[8], D.I. Futyan[16], P. Gagnon[7], J.W. Gary[4], J. Gascon[18], S.M. Gascon-Shotkin[17], N.I. Geddes[20], C. Geich-Gimbel[3], T. Geralis[20], G. Giacomelli[2], P. Giacomelli[4], R. Giacomelli[2], V. Gibson[5], W.R. Gibson[13], D.M. Gingrich[30,a], D. Glenzinski[9], J. Goldberg[22], M.J. Goodrick[5], W. Gorn[4], C. Grandi[2], E. Gross[26], J. Grunhaus[23], M. Gruwé[8], C. Hajdu[32], G.G. Hanson[12], M. Hansroul[8], M. Hapke[13], C.K. Hargrove[7], P.A. Hart[9], C. Hartmann[3], M. Hauschild[8], C.M. Hawkes[5], R. Hawkings[27], R.J. Hemingway[6], M. Herndon[17], G. Herten[10], R.D. Heuer[8], M.D. Hildreth[8], J.C. Hill[5], S.J. Hillier[1], P.R. Hobson[25], R.J. Homer[1], A.K. Honma[28,a], D. Horváth[32,c], K.R. Hossain[30], R. Howard[29], P. Hüntemeyer[27], D.E. Hutchcroft[5], P. Igo-Kemenes[11], D.C. Imrie[25], M.R. Ingram[16], K. Ishii[24], A. Jawahery[17], P.W. Jeffreys[20], H. Jeremie[18], M. Jimack[1], A. Joly[18], C.R. Jones[5], G. Jones[16], M. Jones[6], U. Jost[11], P. Jovanovic[1], T.R. Junk[8], D. Karlen[6], V. Kartvelishvili[16], K. Kawagoe[24], T. Kawamoto[24], P.I. Kayal[30], R.K. Keeler[28], R.G. Kellogg[17], B.W. Kennedy[20], J. Kirk[29], A. Klier[26], S. Kluth[8], T. Kobayashi[24], M. Kobel[10], D.S. Koetke[6], T.P. Kokott[3], M. Kolrep[10], S. Komamiya[24], T. Kress[11], P. Krieger[6], J. von Krogh[11], P. Kyberd[13], G.D. Lafferty[16], R. Lahmann[17], W.P. Lai[19], D. Lanske[14], J. Lauber[15], S.R. Lautenschlager[31], J.G. Layter[4], D. Lazic[22], A.M. Lee[31], E. Lefebvre[18], D. Lellouch[26], J. Letts[12], L. Levinson[26], S.L. Lloyd[13], F.K. Loebinger[16], G.D. Long[28], M.J. Losty[7], J. Ludwig[10], A. Macchiolo[2], A. Macpherson[30], M. Mannelli[8], S. Marcellini[2], C. Markus[3], A.J. Martin[13], J.P. Martin[18], G. Martinez[17], T. Mashimo[24], P. Mättig[3], W.J. McDonald[30], J. McKenna[29], E.A. Mckigney[15], T.J. McMahon[1], R.A. McPherson[8], F. Meijers[8], S. Menke[3], F.S. Merritt[9], H. Mes[7], J. Meyer[27], A. Michelini[2], G. Mikenberg[26], D.J. Miller[15], A. Mincer[22,e], R. Mir[26], W. Mohr[10], A. Montanari[2], T. Mori[24], M. Morii[24], U. Müller[3], S. Mihara[24], K. Nagai[26], I. Nakamura[24], H.A. Neal[8], B. Nellen[3], R. Nisius[8], S.W. O'Neale[1], F.G. Oakham[7], F. Odorici[2], H.O. Ogren[12], A. Oh[27], N.J. Oldershaw[16], M.J. Oreglia[9], S. Orito[24], J. Pálinkás[33,d], G. Pásztor[32], J.R. Pater[16], G.N. Patrick[20], J. Patt[10], M.J. Pearce[1], R. Perez-Ochoa8, S. Petzold[27], P. Pfeifenschneider[14], J.E. Pilcher[9], J. Pinfold[30], D.E. Plane[8], P. Poffenberger[28], B. Poli[2], A. Posthaus[3], D.L. Rees[1], D. Rigby[1], S. Robertson[28], S.A. Robins[22], N. Rodning[30], J.M. Roney[28], A. Rooke[15], E. Ros[8], A.M. Rossi[2], P. Routenburg[30], Y. Rozen[22], K. Runge[10], O. Runolfsson[8], U. Ruppel[14], D.R. Rust[12], R. Rylko[25], K. Sachs[10], T. Saeki[24], E.K.G. Sarkisyan[23], C. Sbarra[29], A.D. Schaile[34], O. Schaile[34], F. Scharf[3], P. Scharff-Hansen[8], P. Schenk[34], J. Schieck[11], P. Schleper[11], B. Schmitt[8], S. Schmitt[11], A. Schöning[8], M. Schröder[8], H.C. Schultz-Coulon[10], M. Schumacher[3], C. Schwick[8], W.G. Scott[20], T.G. Shears[16], B.C. Shen[4], C.H. Shepherd-Themistocleous[8],

P. Sherwood[15], G.P. Siroli[2], A. Sittler[27], A. Skillman[15], A. Skuja[17], A.M. Smith[8], G.A. Snow[17], R. Sobie[28], S. Söldner-Rembold[10], R.W. Springer[30], M. Sproston[20], K. Stephens[16], J. Steuerer[27], B. Stockhausen[3], K. Stoll[10], D. Strom[19], P. Szymanski[20], R. Tafirout[18], S.D. Talbot[1], S. Tanaka[24], P. Taras[18], S. Tarem[22], R. Teuscher[8], M. Thiergen[10], M.A. Thomson[8], E. von Törne[3], S. Towers[6], I. Trigger[18], Z. Trócsányi[33], E. Tsur[23], A.S. Turcot[9], M.F. Turner-Watson[8], P. Utzat[11], R. Van Kooten[12], M. Verzocchi[10], P. Vikas[18], E.H. Vokurka[16], H. Voss[3], F. Wäckerle[10], A. Wagner[27], C.P. Ward[5], D.R. Ward[5], P.M. Watkins[1], A.T. Watson[1], N.K. Watson[1], P.S. Wells[8], N. Wermes[3], J.S. White[28], B. Wilkens[10], G.W. Wilson[27], J.A. Wilson[1], G. Wolf[26], T.R. Wyatt[16], S. Yamashita[24], G. Yekutieli[26], V. Zacek[18], D. Zer-Zion[8]

[1]School of Physics and Space Research, University of Birmingham, Birmingham B15 2TT, UK
[2]Dipartimento di Fisica dell' Università di Bologna and INFN, I-40126 Bologna, Italy
[3]Physikalisches Institut, Universität Bonn, D-53115 Bonn, Germany
[4]Department of Physics, University of California, Riverside CA 92521, USA
[5]Cavendish Laboratory, Cambridge CB3 0HE, UK
[6] Ottawa-Carleton Institute for Physics, Department of Physics, Carleton University, Ottawa, Ontario K1S 5B6, Canada
[7]Centre for Research in Particle Physics, Carleton University, Ottawa, Ontario K1S 5B6, Canada
[8]CERN, European Organisation for Particle Physics, CH-1211 Geneva 23, Switzerland
[9]Enrico Fermi Institute and Department of Physics, University of Chicago, Chicago IL 60637, USA
[10]Fakultät für Physik, Albert Ludwigs Universität, D-79104 Freiburg, Germany
[11]Physikalisches Institut, Universität Heidelberg, D-69120 Heidelberg, Germany
[12]Indiana University, Department of Physics, Swain Hall West 117, Bloomington IN 47405, USA
[13]Queen Mary and Westfield College, University of London, London E1 4NS, UK
[14]Technische Hochschule Aachen, III Physikalisches Institut, Sommerfeldstrasse 26-28, D-52056 Aachen, Germany
[15]University College London, London WC1E 6BT, UK
[16]Department of Physics, Schuster Laboratory, The University, Manchester M13 9PL, UK
[17]Department of Physics, University of Maryland, College Park, MD 20742, USA
[18]Laboratoire de Physique Nucléaire, Université de Montréal, Montréal, Quebec H3C 3J7, Canada
[19]University of Oregon, Department of Physics, Eugene OR 97403, USA
[20]Rutherford Appleton Laboratory, Chilton, Didcot, Oxfordshire OX11 0QX, UK
[22]Department of Physics, Technion-Israel Institute of Technology, Haifa 32000, Israel
[23]Department of Physics and Astronomy, Tel Aviv University, Tel Aviv 69978, Israel
[24]International Centre for Elementary Particle Physics and Department of Physics, University of Tokyo, Tokyo 113, and Kobe University, Kobe 657, Japan
[25]Brunel University, Uxbridge, Middlesex UB8 3PH, UK
[26]Particle Physics Department, Weizmann Institute of Science, Rehovot 76100, Israel
[27]Universität Hamburg/DESY, II Institut für Experimental Physik, Notkestrasse 85, D-22607 Hamburg, Germany
[28]University of Victoria, Department of Physics, P O Box 3055, Victoria BC V8W 3P6, Canada
[29]University of British Columbia, Department of Physics, Vancouver BC V6T 1Z1, Canada

[30]University of Alberta, Department of Physics, Edmonton AB T6G 2J1, Canada
[31]Duke University, Dept of Physics, Durham, NC 27708-0305, USA
[32]Research Institute for Particle and Nuclear Physics, H-1525 Budapest, P O Box 49, Hungary
[33]Institute of Nuclear Research, H-4001 Debrecen, P O Box 51, Hungary
[34]Ludwigs-Maximilians-Universität München, Sektion Physik, Am Coulombwall 1, D-85748 Garching, Germany

[a] and at TRIUMF, Vancouver, Canada V6T 2A3
[b] and Royal Society University Research Fellow
[c] and Institute of Nuclear Research, Debrecen, Hungary
[d] and Department of Experimental Physics, Lajos Kossuth University, Debrecen, Hungary
[e] and Department of Physics, New York University, NY 1003, USA

1 Introduction

A large number of studies of inclusive vector-meson production in multihadronic Z^0 decay have so far concentrated on the measurement of fragmentation functions and total inclusive rates (see for example [1] and [2] for reviews and data compilations). Relatively little has been done to investigate the role of meson spin in the production dynamics. The primary quarks from Z^0 decay at LEP are highly polarized, and this may play a role in determining the helicities of leading vector mesons. Measurements of B^* mesons [3–6] have shown that these are produced equally in all three helicity states, as would be expected in a simple statistical picture [7, 8] where sea quark helicities are chosen at random and the ratio of vector to pseudoscalar meson production is 3:1. However, in production of D^* and $\phi(1020)$ mesons at large momentum fraction x_p ($\equiv p_{\mathrm{meson}}/p_{\mathrm{beam}}$), where the mesons have a high probability to contain a primary quark, OPAL have reported [6] deviations from equal populations of the three helicity states. The helicity density matrix element ρ_{00} was found to be greater than 1/3, corresponding to the helicity-zero state being favoured. At the same time, the data showed evidence for negative values of the matrix element $\mathrm{Re}\,\rho_{1-1}$ for both D^* and $\phi(1020)$, in agreement with qualitative predictions of a model based on coherent (non-independent) fragmentation of the primary quark and antiquark [9]. Recently, DELPHI [10] have reported measurements for $\rho(770)^0$, $K^*(892)^0$ and $\phi(1020)$, confirming the OPAL observations of vector-meson spin alignment at large x_p, but finding no evidence for non-zero values of the off-diagonal element $\mathrm{Re}\,\rho_{1-1}$. In the present paper, the OPAL studies are extended to the $K^*(892)^0$ meson (and its antiparticle) in its $K^+\pi^-$ ($K^-\pi^+$) decay mode, and the helicity density matrix elements are measured with high statistics over the entire x_p range. The findings are compared with a new theory [11] based on a Standard Model description of the spin structure of the reaction $e^+e^- \to Z^0 \to q\bar{q}$, followed by coherent fragmentation of the $q\bar{q}$ pair.

2 Formalism for the helicity density matrix

The formalism of the helicity density matrix and its measurement using the vector-meson decay angular distribution have been described fully in [6]. The analysis is done in the vector-meson helicity rest frame, where the z-axis is the direction of the K^{*0} in the overall centre-of-mass system (the same as the laboratory at LEP), the y-axis is the vector product of this z-axis with the incident e^- beam direction, and the x-axis is such as to form a right-handed coordinate system. The angles θ_H and ϕ_H are the usual polar and azimuthal angles of the $K^\pm$ from the K^{*0} decay, measured in this frame. The helicity density matrix elements, $\rho_{\lambda\lambda'}$, are determined by fitting the observed angular distributions W using:

$$W(\cos\theta_{\mathrm{H}}) = \frac{3}{4}\ \left[(1-\rho_{00}) + (3\rho_{00}-1)\cos^2\theta_{\mathrm{H}}\right] \tag{1}$$

$$W(|\alpha|) = (2/\pi)\ [1 + 2\,\mathrm{Re}\,\rho_{1-1}\cos 2|\alpha|\ ] \tag{2}$$

$$W(|\beta|) = (2/\pi)\ [1 + 2\,\mathrm{Im}\,\rho_{1-1}\cos 2|\beta|\ ] \tag{3}$$

The angles α and β are introduced to exploit the symmetry properties of the distributions and, with ϕ defined over the range $-\pi$ to π, are given by: $\alpha = |\phi_{\mathrm{H}}| - \pi/2$; $\beta = |\phi_{\mathrm{H}} + \pi/4| - \pi/2$ for $\phi_{\mathrm{H}} < 3\pi/4$; and $\beta = |\phi_{\mathrm{H}} - 3\pi/4| - \pi/2$ for $\phi_{\mathrm{H}} > 3\pi/4$. Two measured asymmetries give other combinations of matrix elements:

$$\mathrm{Re}\,(\rho_{10}-\rho_{0-1}) = -\frac{\pi}{2\sqrt{2}}\,\frac{N(\sin 2\theta_{\mathrm{H}}\cos\phi_{\mathrm{H}}>0)-N(\sin 2\theta_{\mathrm{H}}\cos\phi_{\mathrm{H}}<0)}{N(\sin 2\theta_{\mathrm{H}}\cos\phi_{\mathrm{H}}>0)+N(\sin 2\theta_{\mathrm{H}}\cos\phi_{\mathrm{H}}<0)} \qquad (4)$$

$$\mathrm{Im}\,(\rho_{10}-\rho_{0-1}) = \frac{\pi}{2\sqrt{2}}\,\frac{N(\sin 2\theta_{\mathrm{H}}\sin\phi_{\mathrm{H}}>0)-N(\sin 2\theta_{\mathrm{H}}\sin\phi_{\mathrm{H}}<0)}{N(\sin 2\theta_{\mathrm{H}}\sin\phi_{\mathrm{H}}>0)+N(\sin 2\theta_{\mathrm{H}}\sin\phi_{\mathrm{H}}<0)} \qquad (5)$$

where N is the number of events in the given angular range.

The element ρ_{00} of the helicity density matrix gives the relative intensity of mesons in the helicity 0 state, while the off-diagonal element ρ_{1-1} is a measure of coherence between the helicity $+1$ and helicity -1 states.

3 The OPAL detector and data samples

The OPAL detector is described in [12]. For the present analysis, the most important components were the central tracking chambers which consist of two layers of silicon microvertex detectors [13], a high-precision vertex drift chamber, a large-volume jet chamber, and a set of drift chambers (the z-chambers) which measure the coordinates of tracks along the direction of the beam. The OPAL coordinate system is defined with the z-axis following the electron beam direction; the polar angle θ is defined relative to this axis, and r and ϕ are the usual cylindrical polar coordinates. The central chambers lie within a homogeneous axial magnetic field of 0.435 T. Charged particle tracking is possible over the range $|\cos\theta| < 0.98$ for the full range of azimuthal angles. For $\mathrm{K}\pi$ systems around the K^{*0} mass, the mass resolution of the detector varies, with momentum, from about 5 to 20 MeV. The OPAL jet chamber is capable of measuring specific energy loss, $\mathrm{d}E/\mathrm{d}x$, with a resolution, $\sigma(\mathrm{d}E/\mathrm{d}x)/(\mathrm{d}E/\mathrm{d}x)$, of 3.5% for well-reconstructed, high-momentum tracks in multihadronic events [14].

The present analysis used the full OPAL sample of 4.3 million multihadronic Z^0 decays recorded at LEP 1 between 1990 and 1995. To correct for losses due to the acceptance and efficiency of the experiment and the selection procedures, and also to provide signal and background shapes for fits to the data mass spectra, 6 million Monte Carlo events were used, which had been generated using JETSET 7.4 [15] tuned to the OPAL data [16], and processed through a full simulation of the experiment [17] and the data reconstruction and analysis.

A detailed description of the selection of hadronic Z^0 decay events in OPAL is given in [18]. For the present analysis, tracks in the selected events were required to have: a minimum momentum transverse to the beam direction of 150 MeV/c; a maximum momentum of $1.07\times E_{\mathrm{beam}}$, based on the the momentum resolution of the detector; a distance of closest approach to the interaction point less than 5 cm in the plane orthogonal to the beam direction, and the corresponding distance along the beam direction less than 40 cm; a first measured point within a radius of 75 cm from the vertex; and at least 20 hits available for measurement of specific energy loss, $\mathrm{d}E/\mathrm{d}x$.

Kaons and pions were identified using the $\mathrm{d}E/\mathrm{d}x$ measurements. For each track, a χ^2 probability (weight) was formed for each of the stable particle hypotheses (e, μ, π, K and p). A track was identified as a pion or a kaon if the appropriate weight was above 5% and was larger than the weight for each of the other stable hadron hypotheses. Between momenta of 0.8 and

2.0 GeV/c, the π, K and p bands overlap in $\mathrm{d}E/\mathrm{d}x$, leading to considerable ambiguity among hypotheses. Therefore no tracks were identified as kaons in this momentum range although, since most tracks are pions, pion identification was still allowed. With these $\mathrm{d}E/\mathrm{d}x$ selections, pions were identified with a typical efficiency of 50% and a sample purity of 90% over most of the momentum range. The kaon efficiency was around 45%, while the sample purity was typically 30% at low momentum, rising to 50% at high momentum.

4 Measurement of the $\mathrm{K}^*(892)^0$ helicity density matrix and fragmentation function

4.1 Inclusive $\mathrm{K}^\pm\pi^\mp$ mass spectra

For both the real and simulated data samples, inclusive mass spectra were formed for $\mathrm{K}^\pm\pi^\mp$ and $\mathrm{K}^\pm\pi^\pm$ systems in ranges of scaled momentum, x_p, of the 2-particle systems. Within each of 12 x_p ranges, whose limits are given in table 1, the data were further divided, based on the $\mathrm{K}^\pm$ direction in the $\mathrm{K}\pi$ helicity frame, into each of six bins of $\cos\theta_\mathrm{H}$, four bins of $|\alpha|$, four bins of $|\beta|$ and, for asymmetry measurements, the positive and negative regions of each of $\sin 2\theta_\mathrm{H}\cos\phi_\mathrm{H}$ and $\sin 2\theta_\mathrm{H}\sin\phi_\mathrm{H}$. This resulted in $12 \times 18 = 216$ mass spectra for each of $\mathrm{K}^\pm\pi^\mp$ and $\mathrm{K}^\pm\pi^\pm$. To account for combinatorial backgrounds, some of which change rapidly near the K^{*0} peak region due to kinematics, background-subtracted mass spectra were formed by subtracting the like-charge $\mathrm{K}^\pm\pi^\pm$ spectra from those for $\mathrm{K}^\pm\pi^\mp$. For the Monte Carlo sample, separate spectra were also made for the most important states contributing to $\mathrm{K}^\pm\pi^\mp$, using information on the origin of each track at the generator level.

Imperfect particle identification leads to significant contributions in the $\mathrm{K}^\pm\pi^\mp$ mass spectra from $\pi^+\pi^-$. The $\rho(770)^0$ reflection is particularly important. For kinematical reasons, its shape and peak position vary with x_p and with the reconstructed $\cos\theta_\mathrm{H}$ of the misidentified pion. In general, the ρ^0 reflection peaks well above the mass of the K^{*0} for negative values of $\cos\theta_\mathrm{H}$ but moves under the K^{*0} peak as $\cos\theta_\mathrm{H}$ approaches $+1$. Figure 1, which shows the background-subtracted $\mathrm{K}^\pm\pi^\mp$ mass spectra in the six $\cos\theta_\mathrm{H}$ bins for $0.3 < x_p < 0.4$, illustrates this behaviour of the ρ^0 reflection. The $\pi^+\pi^-$ products of the ω decay also peak close to the K^{*0} and move with $\cos\theta_\mathrm{H}$, but they form a broader distribution. Other states, such as $\phi(1020) \to \mathrm{K}^+\mathrm{K}^-$, are less important and are negligible near to the K^{*0} peak when compared to the combinatorial backgrounds.

4.2 Efficiency for K^{*0} reconstruction

The overall reconstruction efficiency for K^{*0} decaying via $\mathrm{K}^\pm\pi^\mp$ was measured separately in each of the 216 bins (of x_p plus an angular variable) using the Monte Carlo simulation. The efficiency typically varied between 10% and 25% with $\cos\theta_\mathrm{H}$ for all x_p above 0.1, while at lower x_p it was a stronger function of $\cos\theta_\mathrm{H}$, varying from 5% to 35%. The efficiency depended much less on the azimuthal angles, α and β.

Due to the track selection and particle identification criteria, and particularly to the fact that no kaons were identified in the overlap region of $\mathrm{d}E/\mathrm{d}x$ from 0.8 to 2 GeV/c, the K^{*0} efficiency was zero for some regions in the x_p versus $\cos\theta_\mathrm{H}$ plane, particularly for $x_p < 0.15$.

The limits of the x_p bins, listed in table 1, were chosen to ensure that each bin of x_p contained a measurable K^{*0} signal for every bin of $\cos\theta_H$. Because the decay particles have a momentum of about 300 MeV/c for a K^{*0} at rest, measurements were possible down to $x_p = 0$.

4.3 Measurements of the helicity density matrix

Each of the 216 background-subtracted mass spectra was fitted using a minimum χ^2 fit, for 100 bins of mass over the range 0.675 – 1.175 GeV, to a sum of contributions (as histograms) from $K^*(892)^0$ signal, $\rho(770)^0$ reflection, $\omega(782)$ reflection and background. For the K^{*0} signal, the shape was taken from the detector-level Monte Carlo simulation, but because the K^{*0} is generated in JETSET as a simple Breit-Wigner resonance, the output of the simulation was reweighted as a function of mass to reproduce a P-wave Breit-Wigner with mass-dependent width, which is expected to represent the K^{*0} line shape in the real data. This procedure automatically takes account of variations of mass resolution with momentum and decay angles. The shapes of the ω reflections were also taken from the simulation. To obtain the shapes of the residual combinatorial backgrounds for the fits, the Monte Carlo spectra were treated in the same way as the data, and then the contributions from K^{*0} and the ρ^0 and ω reflections were removed.

The shape of the $\rho(770)^0$ resonance in Z^0 decay has long been known to be severely distorted from a Breit-Wigner shape [19], particularly at low x_p where the peak mass is shifted by some 40 MeV. The source of the distortion is still uncertain, but is likely to be due to residual Bose-Einstein correlations [20]. The standard implementation of Bose-Einstein correlations in the JETSET program has been found to improve significantly the agreement with data [19, 21]. The ALEPH Collaboration [22] have measured inclusive ρ^0 production by allowing, in their $\pi^+\pi^-$ mass spectrum fits, variation of the JETSET parameters which control the strength of the correlations. As the standard representation of the ρ^0 shape for the present analysis, the fitted ALEPH values have been used to generate ρ^0 line shapes using JETSET. Since the Bose-Einstein effects act primarily on low-momentum particles, shapes were generated as functions of both x_p and $\cos\theta_H$ since for a given value of x_p the momentum of a decay pion is related to $\cos\theta_H$. As a result the line shape of the ρ^0, and consequently its reflection in $K^\pm\pi^\mp$, varies with both x_p and $\cos\theta_H$. To obtain the shapes of the reflections in $K^\pm\pi^\mp$, the decay tracks from the generated ρ^0 mesons were passed through a Monte Carlo model with a simplified simulation of the detector and the analysis selections. The performance of this simulation was verified by comparing its results, for a simple Breit-Wigner shape as input, with the output of the full detector-level JETSET simulation. Other possible ρ^0 line shapes were considered for studies of systematic errors, and will be discussed in section 5.1.

Figure 1 shows, as an example, the results of the mass spectrum fits for the six bins of $\cos\theta_H$ in the x_p bin $0.3 < x_p < 0.4$. The average value of χ^2 for the fits, all of which were acceptable, to the 72 independent mass spectra in bins of $\cos\theta_H$ and x_p was 99.2 for 96 degrees of freedom. The K^{*0} intensities extracted from the fits were fully corrected for efficiency and branching ratio to give, in each of the 12 bins of x_p, the three inclusive double differential cross sections for K^{*0} production and decay, $(1/\sigma_h)\mathrm{d}^2\sigma/\mathrm{d}x_p\mathrm{d}y$, for $y = \cos\theta_H$, $|\alpha|$ and $|\beta|$, where σ_h is the total multihadronic Z^0 cross section.

The helicity density matrix elements in each x_p bin were obtained by fitting these cross sections to the appropriate form (equations (1), (2) and (3)) as functions of the angular variables. Figures 2 and 3 show some of the measured differential cross sections in $\cos\theta_H$ and $|\alpha|$ along with the results of the fits. The two asymmetries, in $\sin 2\theta_{\mathrm{H}} \cos \phi_{\mathrm{H}}$ and $\sin 2\theta_{\mathrm{H}} \sin \phi_{\mathrm{H}}$, were also measured (equations (4) and (5)).

As outlined in section 4.2 the K^{*0} efficiencies were measured for bins of $\cos\theta_{\mathrm{H}}$ and ϕ_{H}, each integrated over the range of the other, using Monte Carlo events which were generated with isotropic decay distributions. Since the data clearly show non-isotropic decay distributions at large x_p, any correlations in efficiency between $\cos\theta_{\mathrm{H}}$ and ϕ_{H} could therefore bias the results of the measurements. The fits were therefore iterated, at each stage using the fitted values of the density matrix elements to generate angular distributions with which to recalculate the efficiencies in $\cos\theta_{\mathrm{H}}$ and ϕ_{H} for the next iteration. The procedure produced only small changes, well within the statistical errors, to the measurements. The final results quoted are those obtained for two iterations, after which no further changes were induced within the quoted number of significant figures.

The measured values of $\mathrm{Im}\,\rho_{1-1}$, $\mathrm{Re}\,(\rho_{10}-\rho_{0-1})$ and $\mathrm{Im}\,(\rho_{10}-\rho_{0-1})$ were found, as expected, to be consistent with zero over the entire x_p range, with weighted average values for $x_p > 0.3$ of -0.03 ± 0.03, -0.06 ± 0.05 and -0.02 ± 0.04 respectively. For $x_p < 0.3$ the values of ρ_{00} and $\mathrm{Re}\,\rho_{1-1}$ were also consistent with an isotropic decay distribution. However in the large momentum region, $x_p > 0.3$, the diagonal element ρ_{00} was found to be larger than 1/3 while $\mathrm{Re}\,\rho_{1-1}$ was negative. Table 1 gives the measured values of ρ_{00} and $\mathrm{Re}\,\rho_{1-1}$ in the bins of x_p. Systematic errors, given in the table, are discussed below in section 5. The data are also shown in figure 4 where the clear deviations from $\rho_{00}= 1/3$ and $\mathrm{Re}\,\rho_{1-1}= 0$ are seen for $x_p > 0.3$, indicative of a 'leading particle effect', i.e. the probability for the meson to contain one of the primary quarks rises as the scaled momentum increases; this is discussed further in section 6.

4.4 Fragmentation function and total rate

For each of the 12 x_p bins, the fragmentation function, $(1/\sigma_{\mathrm{h}})\mathrm{d}\sigma/\mathrm{d}x_p$, was measured by integrating the fitted curves obtained from the $\cos\theta_{\mathrm{H}}$ spectra. The results are given in table 1. The total inclusive rate for K^{*0} production was obtained by integrating the fragmentation function. Since the differential cross section has been measured over the entire x_p range, no explicit systematic uncertainty arises from extrapolation using a Monte Carlo model. However there is an implicit assumption, borne out by the measurements, that the angular distribution in the Monte Carlo model is the same as that for the data for $0.03 < x_p < 0.1$ where there is a significant region of zero efficiency in the $\cos\theta_{\mathrm{H}}$ versus x_p plane. The overall inclusive rate was determined to be $0.74 \pm 0.02 \pm 0.02$ $\mathrm{K}^*(892)^0$ mesons per multihadronic Z^0 decay, in agreement with previous measurements [22–24] (but with smaller statistical and systematic errors). These results update the previous OPAL measurements [23] of the $\mathrm{K}^*(892)^0$ fragmentation function and total inclusive rate. Since the present measurements have been obtained by integrating the cross section, $(1/\sigma_{\mathrm{h}})\mathrm{d}^2\sigma/\mathrm{d}x_p\mathrm{d}\cos\theta_{\mathrm{H}}$, they are in principle more accurate at large x_p than all previous measurements; in previous analyses the data were not binned in $\cos\theta_{\mathrm{H}}$, and efficiencies were calculated assuming isotropic decay distributions.

5 Systematic effects

5.1 The $\rho(770)^0$ line shape

An important source of systematic error on the K^{*0} measurements clearly arises from uncertainty in the shape of the $\rho(770)^0$ resonance and its reflection in the $K^{\pm}\pi^{\mp}$ mass spectrum. To measure the systematic error from this source, the fits were repeated using two extreme possibilities for the shapes: those obtained from the simple Breit-Wigner resonance in the full detector-level simulation; and shapes obtained by multiplying a relativistic P-wave Breit-Wigner with a skewing factor which varied with x_p, as used in [20,23]. The former shape has no skewing of the line shape and is known to give poor fits to the $\pi^+\pi^-$ mass spectra, particularly at low x_p. The latter includes a shift of the peak position and a skewing of the line shape to low masses, but produces too sharp a cut-off at high mass. Because the ρ^0 reflection is more important at $\cos\theta_{\mathrm{H}} > 0$, the entire analysis was also repeated using only the negative region of $\cos\theta_{\mathrm{H}}$. For each of the measurements of inclusive cross sections and helicity density matrix elements the systematic error from the ρ^0 lineshape uncertainty was taken to be $1/\sqrt{12}$ times twice the maximum deviation obtained from the standard fit value.

5.2 Detector and $\mathrm{d}E/\mathrm{d}x$ simulation

The analysis was repeated, dividing the data into two approximately equal samples covering two ranges of K^{*0} production angle: $|\cos\theta| < 0.5$ and $|\cos\theta| > 0.5$. Here θ is the angle between the $K^{\pm}\pi^{\mp}$ system and the incident electron beam. The former range is entirely in the barrel region of OPAL, while the latter covers part of the barrel plus the whole of the end cap regions. In the barrel region, tracks may have the maximum number of jet chamber hits; at higher values of $|\cos\theta|$ the number of possible hits falls and the systematics of $\mathrm{d}E/\mathrm{d}x$ measurements change due to the low angle of the tracks with respect to the wires of the jet chamber. As well as serving as a check for any systematic differences arising from the detector simulation of these two regions, this analysis provided results for comparison with theoretical predictions (see section 6). The measurements of the cross sections and ρ_{00} values were in good agreement for the two regions, within the statistical errors, and so no systematic errors were assigned from this study. The values of $\mathrm{Re}\,\rho_{1-1}$ may be expected to vary with $\cos\theta$, as will be discussed in section 6.

To investigate further the effects of the $\mathrm{d}E/\mathrm{d}x$ requirements, the minimum number of hits required on a track was doubled to 40, and the analysis repeated, with systematic errors taken to be the maximum deviation of any measurement from its standard fit value.

Further systematic checks on the simulation of the energy loss were made by varying the assumed mean values of the theoretical $\mathrm{d}E/\mathrm{d}x$ distributions for a given track hypothesis, and the assumed resolution on the energy loss measurements. Studies of well-identified pions from K^0_S decays, protons from Λ decays and kaons from D^0 and τ decays were used to place limits on the maximum possible deviations of these quantities, and the analysis was repeated, with the $\mathrm{d}E/\mathrm{d}x$ weights of the tracks being recalculated each time. Systematic errors were again assigned as $1/\sqrt{12}$ times twice the maximum measured deviations from the standard fit values.

5.3 Influence of charm decays

Decays of charmed particles of the type $P \rightarrow K^{*0} + P'$, where P and P′ denote any pseudoscalar mesons (for example $\overline{D^0} \rightarrow K^{*0}\pi^0$), must produce K^{*0} mesons which are in the helicity-zero state when viewed from the P rest frame. The total contribution of all such known decays [25] to the overall K^{*0} spin alignment in the helicity frame has been studied using Monte Carlo and was found to be negligible. Their removal would have no measurable effect below $x_p = 0.2$ and would reduce the measured values of ρ_{00} by a maximum of 0.02 at x_p around 0.5; their effect was therefore ignored.

5.4 The K^{*0} line shape

To take account of possible long tails in the line shape of the K^{*0} resonance beyond the upper limit of the fits to the mass spectra, the relativistic P-wave Breit-Wigner used for the fits was integrated out to ten full widths above the nominal peak position, resulting in an increase of 5% in the total intensity. Since the shape of such a resonance is uncertain so far from the pole position, one half of this extra contribution was added to each measurement of the differential cross section (the results in table 1 already include these corrections), and an additional systematic error of $5\%/\sqrt{12}$ was assigned to each measurement and to the total integrated rate. This systematic error has no influence on the measurements of the spin density matrix elements.

The final systematic errors, as given in table 1, were obtained by combining in quadrature the contributions from all of the above sources. For all of the measurements (of cross sections and spin density matrix elements) the systematic errors from detector and $\mathrm{d}E/\mathrm{d}x$ effects were found to be approximately equal to those from the ρ^0 line shape uncertainties.

6 Comparison of results with theory

In a recent paper [11], a relation is derived between the values of ρ_{00} and $\mathrm{Re}\,\rho_{1-1}$ for vector mesons containing a primary quark, using Standard Model parameters and some plausible assumptions about hadronization. According to this theory, negative values of the off-diagonal element $\mathrm{Re}\,\rho_{1-1}$ are generated for leading vector mesons by coherence in the production and fragmentation of the primary quark and antiquark from the Z^0 decay. For the primary K^{*0} mesons, it is predicted that

$$\mathrm{Re}\ \rho_{1-1} \approx -0.17(1-\rho_{00})\frac{\sin^2\theta}{(1+\cos^2\theta)} \tag{6}$$

where θ is the production angle of the leading K^{*0} relative to the electron beam. In the present analysis, there is no explicit cut on $|\cos\theta|$, although the efficiency falls rapidly for values above 0.9. Based on the distribution of high-x_p K^{*0} production angles in the detector-level Monte Carlo events, the ratio $\mathrm{Re}\rho_{1-1}/(1-\rho_{00})$ is predicted by equation (6) to be approximately -0.10 for mesons containing a primary quark. Table 2 shows the measured values at large x_p, with statistical and systematic errors combined. The results in each independent x_p bin are compatible with the theory, although there is a suggestion that the magnitudes of the measured values are larger than predicted. The weighted average value is -0.19 ± 0.05 for $x_p > 0.3$. It should be noted however that comparison with the theory is somewhat obscured by lack of knowledge of the proportion of K^{*0} mesons which contain a primary quark at a given value of x_p. Studies using the JETSET model suggest that this fraction is around 20% at $x_p = 0.3$, rising approximately linearly to 100% at $x_p = 1$.

As discussed in section 5.2 the density matrix elements were measured separately for two ranges of K^{*0} production angle: $|\cos\theta| < 0.5$ and $|\cos\theta| > 0.5$. The results are given in table 3. The dependence of $\mathrm{Re}\,\rho_{1-1}$ on θ predicted by equation (6) would imply that the ratio of these two measurements should be 2.3, assuming no variation of ρ_{00} with $\cos\theta$. The measured ratio of the weighted mean values is 1.5 ± 0.7 over the range $x_p > 0.3$, consistent within relatively large errors both with the theory and with no variation of $\mathrm{Re}\,\rho_{1-1}$ with $\cos\theta$.

While the theory of [11] derives a relationship between the values of ρ_{00} and $\mathrm{Re}\,\rho_{1-1}$, it does not offer any explanation for deviations of ρ_{00} from 1/3. A number of models relevant to this topic are discussed in [6] and [10]. In the simple statistical model based on spin counting [7], the maximum value of ρ_{00} is 0.5, and this can only occur when there is zero probability for production of pseudoscalar mesons containing the primary quark. While this model fits with the measurements of B^* mesons [3–6], it is now clearly ruled out by the LEP data for the lighter vector mesons. The QCD-inspired model of [26], which predicts $\rho_{00}= 0$ for leading vector mesons is also ruled out by the measurements; however [26] does point out that this result would only be expected in the limit that quark and meson masses and transverse momenta can be neglected. The model of [7], in which vector-meson production is considered as arising from the helicity-conserving process $q \rightarrow qV$, predicts $\rho_{00}= 1$ for the leading vector mesons. Although its result is in accord with the observations, this model is based on a picture of parton hadronization which has been superseded by the more firmly based, detailed and successful string and cluster models; these latter models do not however address the dynamical role of meson spin in the hadronization.

7 Conclusions

From the present analysis, together with OPAL measurements [6] of inclusive ϕ and D^* mesons, and DELPHI [10] measurements of ρ^0, K^{*0} and ϕ, it is now clearly established that leading vector mesons, other than the B^*, are spin-aligned with a preference for the helicity-zero state.

The results of the present K^{*0} analysis are consistent with the idea that coherence in the $q\bar{q}$ production and fragmentation plays a role in generating non-zero values of the off-diagonal element $\mathrm{Re}\,\rho_{1-1}$, in agreement with the theory of [11]. However the measured value of $\mathrm{Re}\,\rho_{1-1}$ for the K^{*0} is slightly larger than the theory predicts, while for the D^* it is smaller [6]. This may indicate a flavour dependence of the mechanism producing the spin alignment, or the existence of more than one mechanism. While OPAL observe non-zero (and negative) values of $\mathrm{Re}\,\rho_{1-1}$ in three separate analyses, of K^{*0}, ϕ and D^* production, the DELPHI results on ρ^0, K^{*0} and ϕ are all consistent with zero, within relatively small errors. Further measurements are required to clear up this apparent inconsistency.

The LUND string model [27], as implemented in the JETSET Monte Carlo program [15], is highly successful in describing many features of hadronic Z^0 decay events [28]. However, in the simplest string model, no spin alignment of vector mesons is expected [27]. Similarly, the QCD cluster model of HERWIG [29] has no mechanism to produce spin-aligned vector mesons; and neither model will generate non-zero values for the off-diagonal elements of the helicity density matrix. The vector meson spin alignment results therefore provide a challenge to the standard Monte Carlo models of the physics of inclusive hadron production in Z^0 decay at LEP. Can they be extended to include a physical mechanism which explains the measured vector-meson helicity density matrices?

Acknowledgements

We particularly wish to thank the SL Division for the efficient operation of the LEP accelerator at all energies and for their continuing close cooperation with our experimental group. We thank our colleagues from CEA, DAPNIA/SPP, CE-Saclay for their efforts over the years on the time-of-flight and trigger systems which we continue to use. In addition to the support staff at our own institutions we are pleased to acknowledge the
Department of Energy, USA,
National Science Foundation, USA,
Particle Physics and Astronomy Research Council, UK,
Natural Sciences and Engineering Research Council, Canada,
Israel Science Foundation, administered by the Israel Academy of Science and Humanities,
Minerva Gesellschaft,
Benoziyo Center for High Energy Physics,
Japanese Ministry of Education, Science and Culture (the Monbusho) and a grant under the Monbusho International Science Research Program,
German Israeli Bi-national Science Foundation (GIF),
Bundesministerium für Bildung, Wissenschaft, Forschung und Technologie, Germany,
National Research Council of Canada,
Hungarian Foundation for Scientific Research, OTKA T-016660, T023793 and OTKA F-023259.

References

[1] A. Böhrer, "Inclusive particle production in hadronic decays of the Z boson at LEP I", preprint CERN-OPEN/96-021, Si-96-15, submitted to Phys. Rep.

[2] G.D. Lafferty, P.I. Reeves and M.R. Whalley, J. Phys. G: Nucl. Part. Phys. 21 (1995) A1-A151.

[3] DELPHI Coll., P. Abreu et al., Z. Phys. C68 (1995) 353.

[4] ALEPH Coll., D. Buskulic et al., Z. Phys. C69 (1995) 393.

[5] OPAL Coll., K. Ackerstaff et al., Z. Phys. C74 (1997) 413.

[6] OPAL Coll., G. Alexander et al., Z. Phys. C74 (1997) 437.

[7] J.F. Donoghue, Phys. Rev. D19 (1979) 2806.

[8] I.I.Y. Bigi, Nuovo Cimento A41 (1977) 581.

[9] M. Anselmino, P. Kroll and B. Pire, Z. Phys. C29 (1985) 135;
A. Anslem, M. Anselmino, F. Murgia and M.G. Ryskin, J. Exp. Th. Phys. 60 (1994) 496.

[10] DELPHI Coll., P. Abreu et al., "Measurement of the spin density matrix for the ρ^0, $K^*(892)$ and ϕ produced in Z decays", preprint CERN-PPE/97-55, submitted to Phys. Lett. B.

[11] M. Anselmino, M. Bertini, F. Murgia and P. Quintairos, "Off-diagonal helicity density matrix elements for vector mesons produced at LEP", preprint hep-ph/9704420, submitted to Z. Phys. C.

[12] OPAL Coll., K. Ahmet et al., Nucl. Instrum. Methods A305 (1991) 275.

[13] P.P. Allport et al., Nucl. Instrum. Methods A324 (1993) 34;
P.P. Allport et al., Nucl. Instrum. Methods A346 (1994) 476.

[14] M. Hauschild et al., Nucl. Instrum. Methods A314 (1992) 74.

[15] T. Sjöstrand, Comp. Phys. Commun. 39 (1986) 347;
T. Sjöstrand and M. Bengtsson, Comp. Phys. Commun. 43 (1987) 367;
T. Sjöstrand, CERN manual CERN-TH.7112/93 (1993) (Geneva, CERN).

[16] OPAL Coll., M.Z. Akrawy et al., Z. Phys. C47 (1990) 505;
The JETSET 7.4 parameters were tuned as described in OPAL Coll., G. Alexander et al., Z. Phys. C69 (1996) 543.

[17] J. Allison et al., Nucl. Instrum. Methods A317 (1992) 47.

[18] OPAL Coll., G. Alexander at al., Z. Phys. C5 (1991) 175.

[19] OPAL Coll., P. D. Acton et al., Z. Phys. C56 (1992) 521.

[20] G.D. Lafferty, Z. Phys. C60 (1993) 659.

[21] DELPHI Coll., P. Abreu et al., Z. Phys. C65 (1994) 587.

[22] ALEPH Coll., D. Buskulic et al., Z. Phys. C69 (1995) 379.

[23] OPAL Coll., R. Akers et al., Z. Phys. C68 (1995) 1.

[24] DELPHI Coll., P. Abreu et al., Z. Phys. C73 (1996) 61.

[25] Particle Data Group, R. M. Barnett et al., Phys. Rev. D54 (1996) 1.

[26] J.E. Augustin and F.M. Renard, N. Phys. B162 (1980) 341.

[27] B. Andersson, G. Gustafson, G. Ingelman and T. Sjöstrand, Phys. Rep. 97 (1983) 31.

[28] I. G. Knowles and G. D. Lafferty, J. Phys. G: Nucl. Part. Phys. 23 (1997) 731.

[29] G. Marchesini et al., Comp. Phys. Commun. 67 (1992) 465.

x_p bin	x_p range	$(1/\sigma_\mathrm{h})\mathrm{d}\sigma/\mathrm{d}x_p$	ρ_{00}	$\mathrm{Re}\,\rho_{1-1}$
1	0.0–0.01	1.22$\pm$ 0.15 $\pm$0.04	0.39$\pm$0.07$\pm$0.13	0.01$\pm$0.06$\pm$0.08
2	0.01–0.03	4.96$\pm$ 0.17 $\pm$0.15	0.29$\pm$0.02$\pm$0.05	0.01$\pm$0.02$\pm$0.03
3	0.03–0.1	4.14$\pm$ 0.20 $\pm$0.19	0.30$\pm$0.03$\pm$0.03	0.02$\pm$0.03$\pm$0.06
4	0.1–0.125	2.35$\pm$ 0.16 $\pm$0.13	0.31$\pm$0.04$\pm$0.06	0.06$\pm$0.04$\pm$0.04
5	0.125–0.14	1.99$\pm$ 0.15 $\pm$0.09	0.29$\pm$0.05$\pm$0.07	$-$0.12$\pm$0.05$\pm$0.07
6	0.14–0.16	1.60$\pm$ 0.11 $\pm$0.10	0.27$\pm$0.05$\pm$0.09	$-$0.03$\pm$0.04$\pm$0.02
7	0.16–0.2	1.30$\pm$ 0.09 $\pm$0.06	0.31$\pm$0.04$\pm$0.05	0.01$\pm$0.03$\pm$0.04
8	0.2–0.3	0.81$\pm$ 0.04 $\pm$0.05	0.34$\pm$0.03$\pm$0.03	$-$0.02$\pm$0.02$\pm$0.01
9	0.3–0.4	0.44$\pm$ 0.03 $\pm$0.03	0.45$\pm$0.03$\pm$0.06	$-$0.13$\pm$0.03$\pm$0.03
10	0.4–0.5	0.22$\pm$ 0.02 $\pm$0.01	0.48$\pm$0.04$\pm$0.04	$-$0.09$\pm$0.04$\pm$0.06
11	0.5–0.7	0.090$\pm$0.009$\pm$0.003	0.53$\pm$0.04$\pm$0.03	$-$0.05$\pm$0.04$\pm$0.02
12	0.7–1.0	0.013$\pm$0.004$\pm$0.003	0.66$\pm$0.09$\pm$0.06	$-$0.08$\pm$0.06$\pm$0.03

Table 1: Inclusive K^{*0} cross sections and helicity density matrix elements measured in the helicity-beam frame over the full range of K^{*0} production angles. The first errors are statistical and the second systematic.

x_p range	$\mathrm{Re}\,\rho_{1-1}/(1-\rho_{00})$
0.3–0.4	-0.24 ± 0.08
0.4–0.5	-0.17 ± 0.13
0.5–0.7	-0.11 ± 0.09
0.7–1.0	-0.24 ± 0.22
0.3–1.0	-0.19 ± 0.05

Table 2: Ratios of K^{*0} helicity density matrix elements measured over the full range of production angles at large x_p. The last row gives the weighted mean value over the range indicated.

x_p range	$\lvert\cos\theta\rvert < 0.5$	$\lvert\cos\theta\rvert > 0.5$
0.3–0.4	-0.12 ± 0.04	-0.13 ± 0.04
0.4–0.5	-0.14 ± 0.06	-0.05 ± 0.06
0.5–0.7	-0.08 ± 0.05	-0.02 ± 0.06
0.7–1.0	-0.17 ± 0.10	-0.01 ± 0.11
0.3–1.0	-0.12 ± 0.03	-0.08 ± 0.03

Table 3: Values of $\mathrm{Re}\,\rho_{1-1}$ measured over different ranges of K^{*0} production angles at large x_p. The last row gives the weighted mean values over the range indicated. Statistical errors only are given; the systematic errors largely cancel when the ratios are taken.

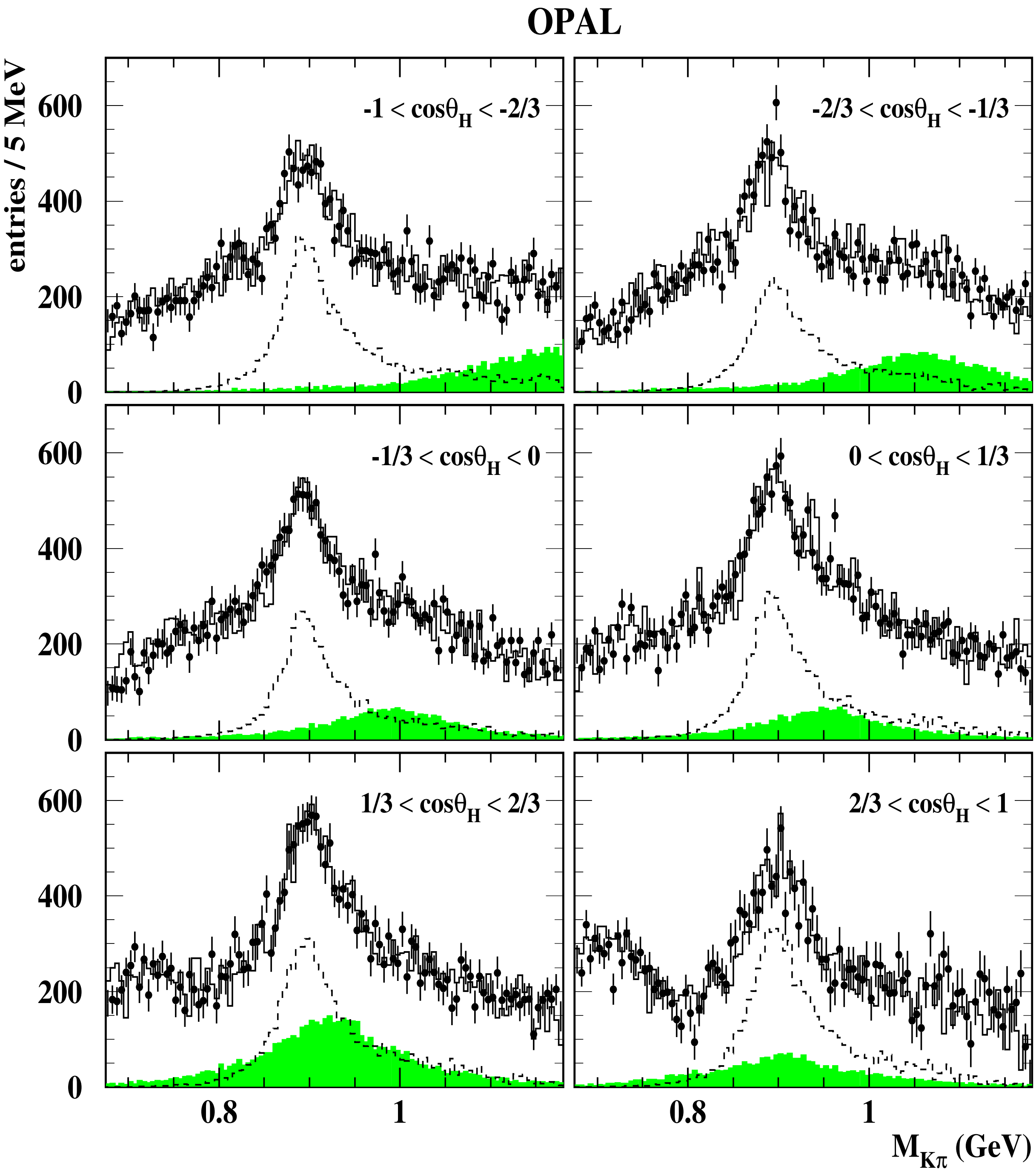

Figure 1: Inclusive background-subtracted $K^{\pm}\pi^{\mp}$ mass spectra for the x_p range $0.3 < x_p < 0.4$ for the 6 bins of $\cos\theta_{\mathrm{H}}$. The points with error bars show the OPAL data. The full histograms show the fits described in section 4.3, with the dashed histograms giving the K^{*0} component and the shaded areas showing the contributions of the ρ^0 reflection.

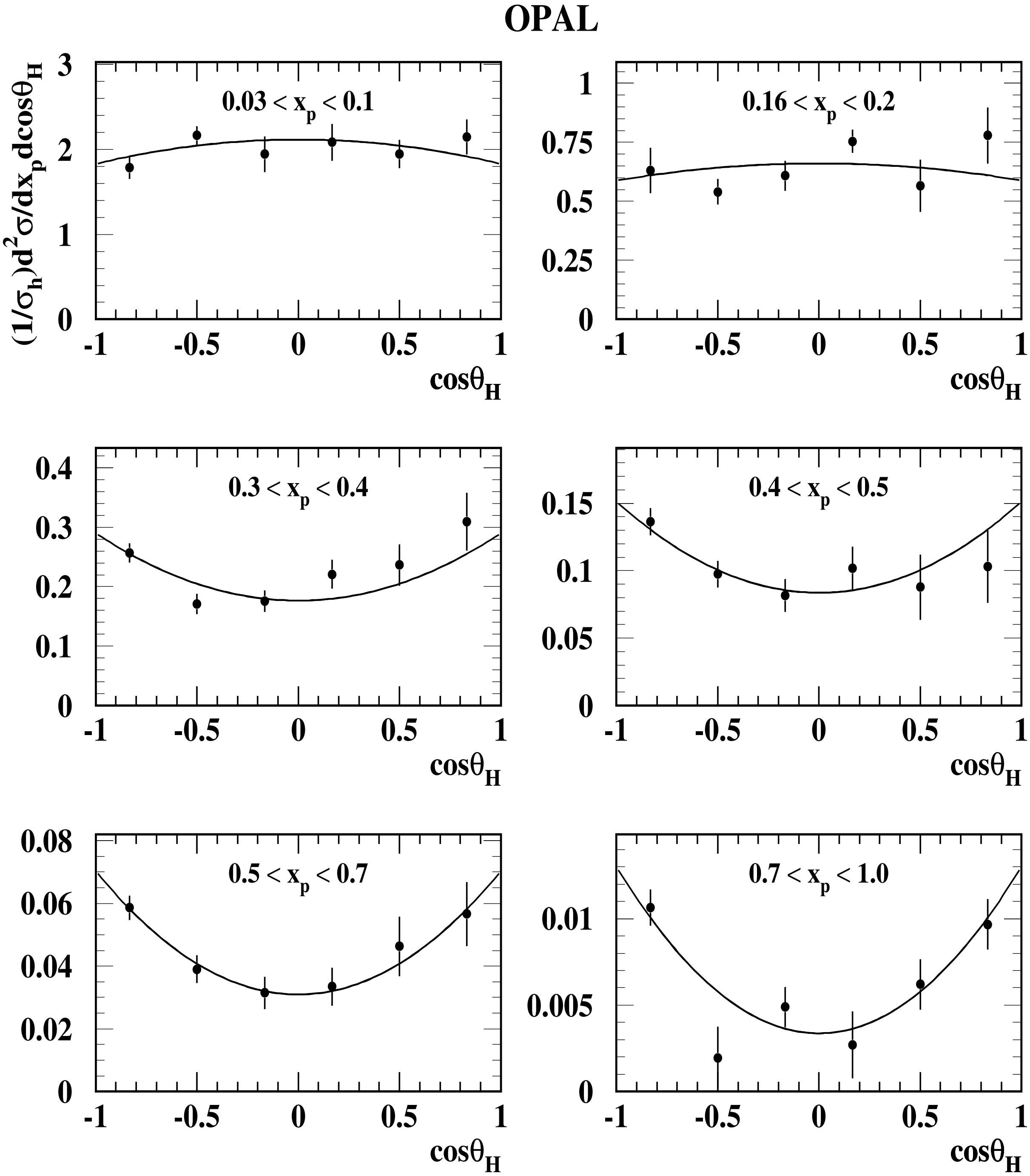

Figure 2: Differential cross sections, $(1/\sigma_{\rm h})\mathrm{d}^2\sigma/\mathrm{d}x_p\mathrm{d}\cos\theta_{\rm H}$, for 6 ranges of x_p. The points are the OPAL data and the curves show the fits used to obtain the helicity density matrix elements ρ_{00}. The errors are statistical only.

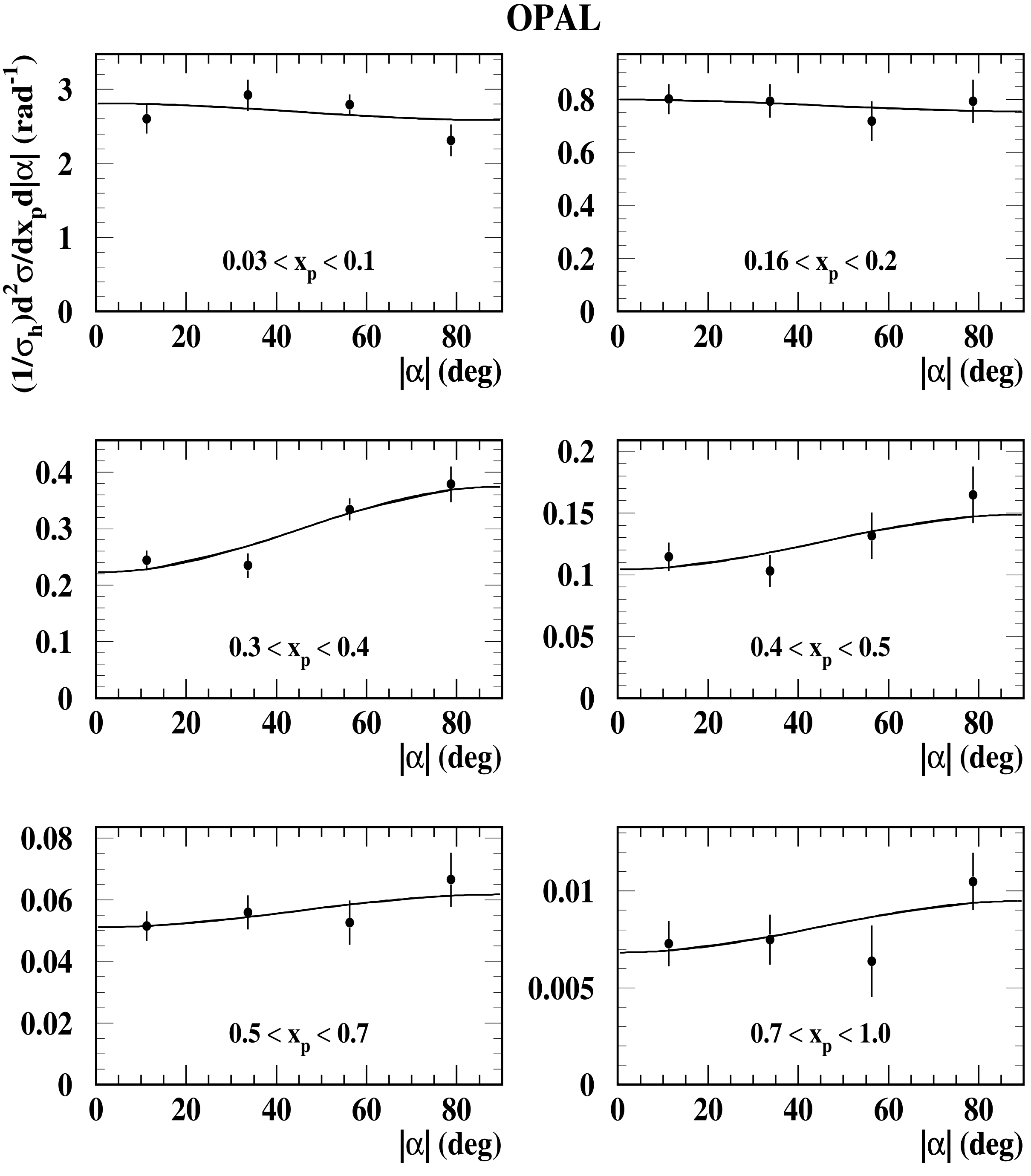

Figure 3: Differential cross sections, $(1/\sigma_{\mathrm{h}})\mathrm{d}^2\sigma/\mathrm{d}x_p\mathrm{d}|\alpha|$, for 6 ranges of x_p. The points are the OPAL data and the curves show the fits used to obtain the helicity density matrix elements $\mathrm{Re}\,\rho_{1-1}$. The errors are statistical only.

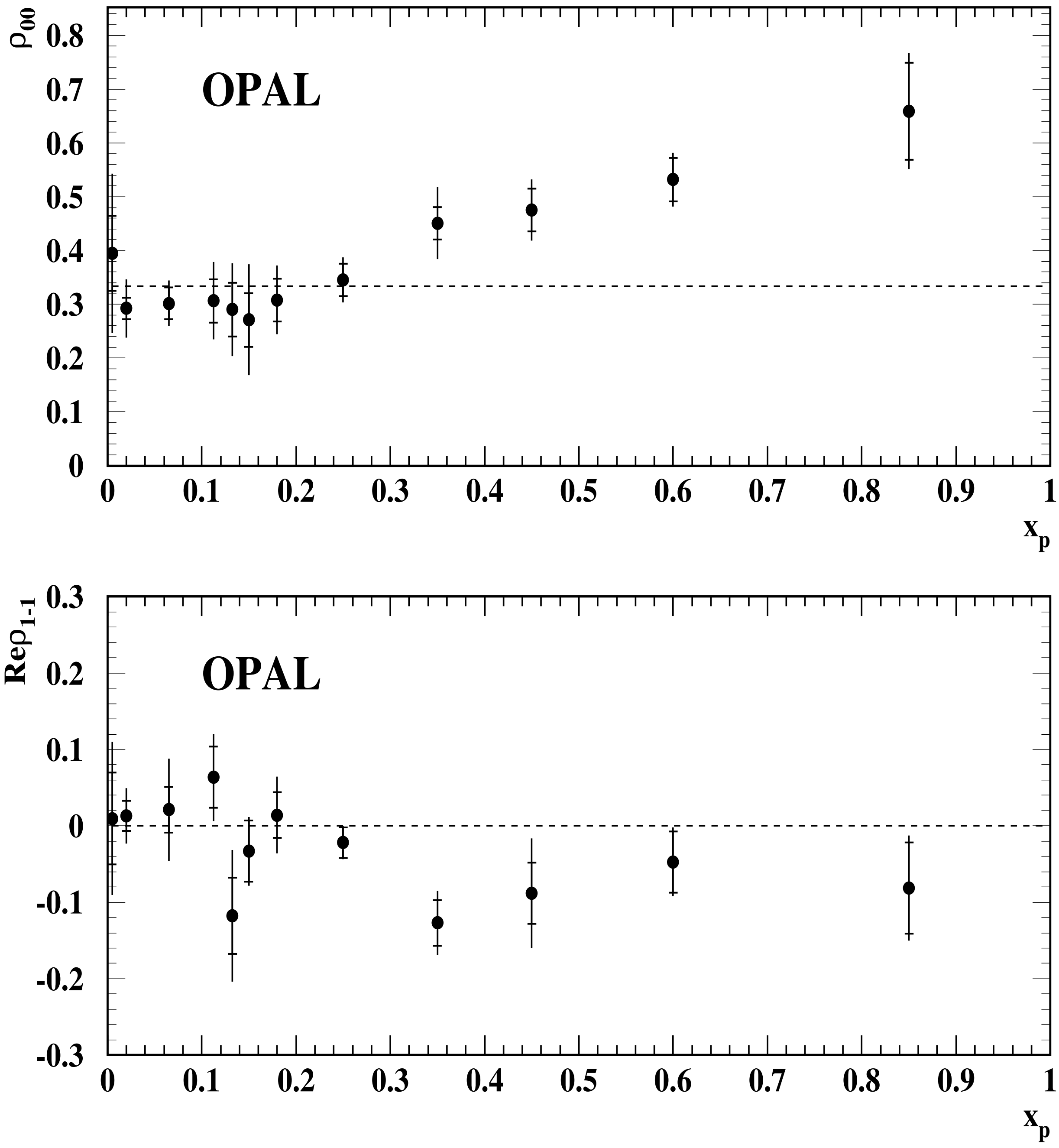

Figure 4: Measured K^{*0} helicity density matrix elements, ρ_{00} and $\mathrm{Re}\,\rho_{1-1}$, as functions of x_p. The error bars are statistical and systematic combined in quadrature, with the tick marks giving the statistical errors only.